Here, we describe a patient with ECHS1 deficiency who presented with Leigh syndrome [MIM #256000] accompanied by hypotonia, metabolic acidosis, and developmental delay. Additionally, the patient presented with combined respiratory chain deficiency, which is not commonly described in most clinical reports of mitochondrial fatty acid β-oxidation disorders. Finally, we discuss the pathology of ECHS1 deficiency and possible interactions between mitochondrial fatty acid β-oxidation and the respiratory chain, which are two important pathways in mitochondrial energy metabolism.

Materials and Methods

This study was approved by the ethical committee of National Center of Neurology and Psychiatry. All the samples in this study were taken and used with informed consent from the family.

Whole-mtDNA Genome Sequence Analysis

Long and accurate PCR amplification of mtDNA followed by direct sequencing was performed according to the previous publication with a slight modification [Matsunaga et al., 2005].

Targeted Exome Sequencing

Almost all exonic regions of 776 nuclear genes (Supp. Table S2), in total 7,368 regions, were sequenced using the Target Enrichment System for next-generation sequencing (HaloPlex; Agilent Technologies, Santa Clara, California, USA) and MiSeq platform (Illumina, San Diego, California, USA). Sequence read alignment was performed with a Burrows–Wheeler Aligner (version 0.6.1) to the human reference genome (version hg19). Realignment and recalibration of base quality scores was performed with the Genome Analysis Toolkit (version 1.6.13). Variants were detected and annotated against dbSNP 135 and 1000 Genomes data (February 2012 release) by Quickannotator.

Sanger Sequencing

Sanger sequencing of candidate genes was performed with the BigDye Terminators v1.1 Cycle Sequencing kit (Thermo Fisher Scientific, Waltham, Massachusetts, USA) as per manufacturer's protocol. Details of primers and conditions are available upon request. DNA sequences from the patients were compared against the RefSeq sequence and the sequences of a healthy control or parents those were sequenced in parallel.

Cell Culture

The patient-derived primary myoblasts were established from the biopsy of patient's skeletal muscle and cultured in DMEM/F-12 (Thermo Fisher Scientific) supplemented with 20% (v/v) heat-inactivated fetal bovine serum (FBS, Thermo Fisher Scientific). DLD-1 (human colon carcinoma) cells were provided by Taiho pharmaceutical company (Tokyo, Japan) and cells were cultured in RPMI-1640 (Thermo Fisher Scientific) supplemented with 10% (v/v) heat-inactivated FBS (Thermo Fisher Scientific). All cells were cultured in 5% CO_2 at 37°C.

Preparation of Mitochondrial Fraction

Mitochondrial fractions from patient's skeletal muscle and patient-derived myoblasts were prepared according to the literature with a slight modification [Frezza et al., 2007].

Immunoblotting

Mitochondrial fraction and protein lysates were prepared from patient's skeletal muscle and patient-derived Myoblasts. Thirty micrograms of protein of mitochondrial fraction or 50 micrograms of protein lysate was separated on 4%–12% Bis-Tris gradient gels (Thermo Fisher Scientific) and transferred to polyvinylidene fluoride membranes. Primary antibodies used were against ECHS1 (Sigma-Aldrich, St. Louis, Missouri, USA), complex II 70 kDa subunit (Abcam, Cambridge, England), β-actin (Santa Cruz, Biotechnology, Dallas, Texas, USA), HA (Wako, Tokyo, Japan), and AcGFP (Thermo Fisher Scientific).

Enzyme Assays

Enzyme activities of mitochondrial respiratory complexes I–V and citrate synthase (CS) were measured in mitochondrial fraction prepared from patient's specimens. The assays for complexes I–IV and CS were performed as described previously [Shimazaki et al., 2012]. The assay for complex V was carried out following the method by Morava and his colleagues with modifications [Morava et al., 2006]. The enoyl-CoA hydratase activity was assayed by the hydration of crotonyl-CoA by a slight modification of the procedure described earlier [Steinman and Hill, 1975]. Five micrograms of protein of the mitochondrial fraction prepared from patient-derived myoblasts was added to 0.3 M Tris–HC1, pH 7.4, containing 5 mM EDTA (Ethylenediaminetetraacetic acid). The reaction was started by the addition of 200 μM crotonyl-CoA and the decrease in absorbance at 280 nm was monitored at 30°C.

Construction of the Immortalized Patient-Derived Myoblasts

The patient-derived myoblasts and control myoblasts were transfected with pEF321-T vector (A kind gift from Dr. Sumio Sugano, University of Tokyo) and the cells were cultured serially for more than ten population doublings until the morphological alteration was observed [Kim et al., 1990].

Expression Vector Preparation and Transfection

For construction of a mammalian expression vector, full-length *ECHS1* (GenBank accession number NM_004092.3) was amplified from a cDNA prepared from control subject using PrimeSTAR GXL DNA polymerase (TaKaRa, Tokyo, Japan). The PCR product was cloned into pEBMulti-Pur (Wako) and the clone was verified by Sanger sequencing. The empty expression vector or an ECHS1 expression vector was transfected into immortalized patient-derived myoblasts using Lipofectamine LTX Reagent (Thermo Fisher Scientific). Each of the two missense variants, c.2T>G; p.M1R and c.5C>T; p.A2V, was independently introduced into the clone by PCR-based site-directed mutagenesis. Each insert with C-terminal HA tag was cloned into pIRES2-AcGFP1 (Clontech Laboratories, Mountain View, California, USA) and the clones were verified by Sanger sequencing. WT and mutant ECHS1 expression vector were transfected into DLD-1 cells using Lipofectamine LTX Reagent (Thermo Fisher Scientific). Twenty-four hours later, the cell lysate was subjected to immunoblotting.

Results

The patient reported here was a boy born to unrelated, healthy parents after a 40-week pregnancy (weight 3,300 g, length 52 cm,

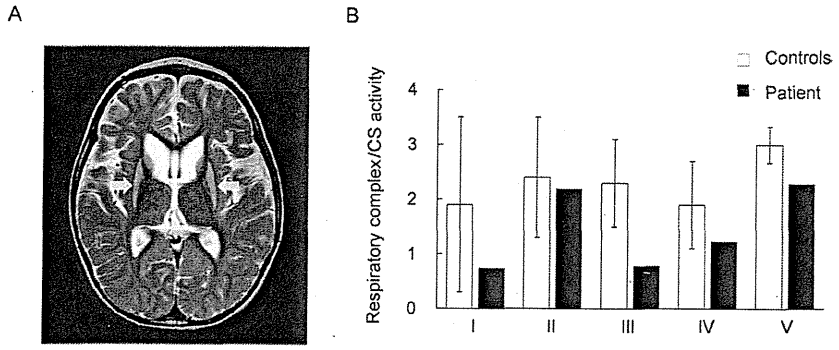

Figure 1. T2-weighted magnetic resonance scan image and enzyme activities of mitochondrial respiratory complexes. **A**: T2-weighted magnetic resonance scan image (MRI) shows bilaterally symmetrical hyperintensities in the putamen (arrows in the image); these are characteristic of Leigh syndrome. **B**: Enzymatic activities of five mitochondrial respiratory complexes (I, II, III, IV, and V) were measured in mitochondrial fractions prepared from the patient's skeletal muscle. Respiratory complexes activities were normalized to citrate synthase activity. Black bars show patient values and white bars show control values. Control values were mean values obtained from five healthy individuals. Patient activity values for complexes I, III, and IV were 39%, 34%, and 64% of the control values, respectively. Error bars represent standard deviations.

Table 1. Urinary Organic Acid Profiling

	Patient RPA (%)	Controls RPA (%)
TCA cycle intermediates		
α-Ketoglutarate	4.52	3.00–102.90
Aconitate	20.37	15.10–86.10
Isocitrate	8.98	8.30–29.00
Other metabolites		
Lactate	11.83[a]	<4.70
Pyruvate	3.18	<24.10
3-Hydroxyisobutyric acid	1.95	<9.00
Methylcitric acid	0.14[a]	Less than trace amount
p-Hydroxy-phenyllactic acid	40.05[a]	<7.00
Glyoxylate	37.71[a]	<6.10

[a]Values outside the normal range.
RPA(%), relative peak area to the area of internal standard (heptadecanoic acid, HDA).

occipitofrontal circumference (OFC) 34.5 cm). Auditory screening test at 2 months of age revealed hearing impairment, and he began to use a hearing aid at 6 months of age. Psychomotor developmental delay was noted at 5 months of age; he could not sit alone, or speak a meaningful word as of 4 years of age. Nystagmus was noted at 10 months of age. Muscle hypotonia, spasticity, and athetotic trunk movement became prominent after 1 year of age. His plasma (20.2 mg/dl) and a cerebrospinal fluid lactate were elevated (25.3 mg/dl, control below 15 mg/dl). Urinary organic acid profiling reveals significantly elevated excretion of glyoxylate (Table 1). Analysis of blood acylcarnitines showed no abnormalities. Brain magnetic resonance scan image showed bilateral T2 hyperintensity of the putamen, typical for Leigh syndrome (Fig. 1A). Because Leigh syndrome is generally caused by defects in the mitochondrial respiratory chain or the pyruvate dehydrogenase complex, we performed a muscle biopsy to measure enzyme activities of mitochondrial respiratory complexes in the patient. Mitochondrial fractions prepared from patient or control specimens were used for all activity measurements. Activity of each respiratory complex was normalized relative to CS activity; normalized values for complexes I, III, and IV activity were decreased to 39%, 34%, and 64% of control values, respectively (Fig. 1B). Moreover, we performed blue native PAGE (BN-PAGE) to examine if the assembly of respiratory complexes were altered in the patient. As a result, there were no clear difference between the patient and the control (Supp. Fig. S1).

Mitochondrial respiratory chain defects can be due to pathogenic mutations in mitochondrial DNA (mtDNA) or nuclear DNA (nDNA) coding for mitochondrial components. Initially, long and accurate PCR amplification of mtDNA followed by direct sequencing was performed and no mutations known to be associated with Leigh syndrome were identified, but previously reported polymorphisms were found (Supp. Table S3). Therefore, to identify the responsible mutations in nDNA, targeted exome sequencing was performed. Coverage was at least 10× for 86.2% of the target regions, and 30× or more for 73.4%. In all, 5,640 potential variants were identified; these included 811 splice-site or nonsynonymous variants. Among those 811 variants, 562 were on the mismapping reads that contained multiple apparent mismatches to the reference DNA sequence. Of the remaining 249 variants, nine that were on target regions with less than 10× coverage were eliminated because data reliability was low. Filtering against dbSNP 135 and 1000 Genomes data, this number was reduced to 13 including compound heterozygous variants in the *ECHS1* [MIM #602292] and 11 heterozygous variants in 11 separate genes (Supp. Table S4). Those variants have been submitted to dbSNP (http://www.ncbi.nlm.nih.gov/SNP/). Because most mitochondrial diseases caused by known nDNA mutations are inherited in an autosomal recessive manner, we focused on the compound heterozygous variants in *ECHS1*—c.2T>G; p.M1R and c.5C>T; p.A2V—as primary candidates.

To confirm the targeted exome sequencing results, we performed Sanger sequencing of genomic *ECHS1* DNA and *ECHS1* cDNA from the patient and his parents. We identified both variants, c.2T>G and c.5C>T, and the respective normal alleles in genomic DNA and cDNA from the patient (Fig. 2A and B) and no other *ECHS1* variants were detected except for common SNPs in the open reading frame. Analysis of genomic DNA from the patient's parents showed that patient's father was heterozygous for only one variant, c.2T>G, and the patient's mother for only the other variant, c.5C>T (Fig. 2A). These results indicated that the patient inherited each variant separately and that both mutant alleles were expressed in the patient (Fig. 2B). Each variant was nonsynonymous and in the region encoding the mitochondrial transit peptide (1–27 amino acids) of ECHS1 [Hochstrasser et al., 1992]; moreover, c.2T>G; p.M1R was a start codon variant (Fig. 2C).

Next, immunoblotting with primary antibodies against ECHS1 was performed to assess protein expression. Mitochondrial

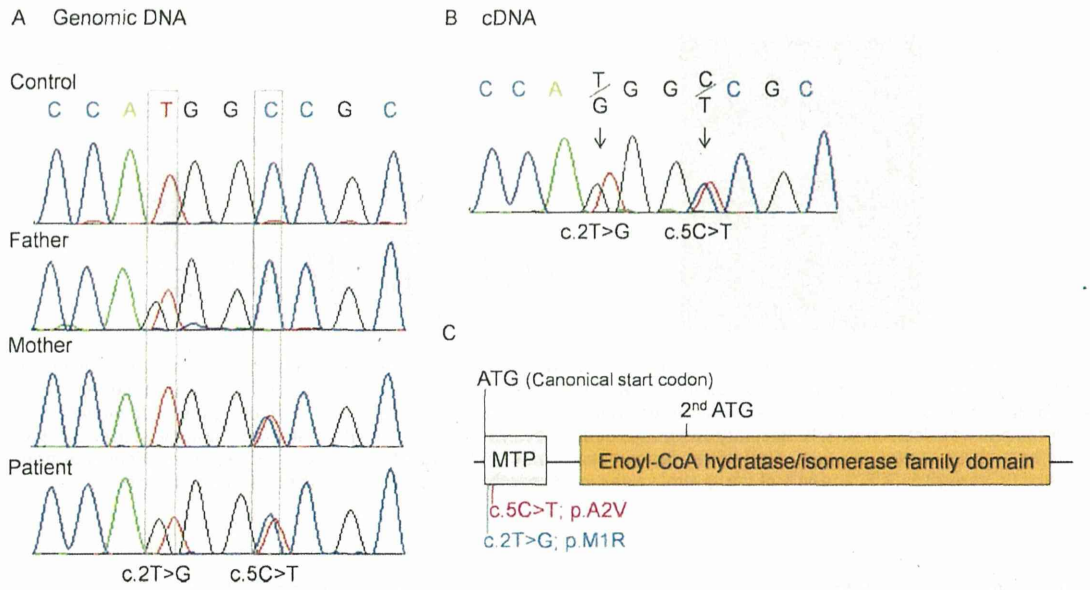

Figure 2. *ECHS1* Sanger sequencing analysis and ECHS1 functional domains. **A**: Sequence chromatograms from part of exon 1 of *ECHS1* were generated by Sanger sequencing of genomic DNA. Each parent had one wild-type allele; the patient's father also harbored a c.2T>G variant, and the patient's mother a c.5C>T variant. The patient inherited each variant allele and was a compound heterozygote. **B**: Sequence chromatograms from part of *ECHS1* exon 1 obtained by Sanger sequencing of cDNA prepared from patient mRNA. The same variants seen in genomic DNA were observed in the cDNA. **C**: A schematic diagram of the functional domains in ECHS1 and the locations of the mutations. MTP, mitochondrial transit peptide.

fractions prepared from patient and control skeletal muscle were used; whole-cell lysates or mitochondrial fractions prepared from patient-derived or control myoblasts were also used. All experiments using these specimens showed that the expression level of ECHS1 protein of the patient was too low to detect by immunoblotting even though the expression level of SDHA was almost the same as controls (Fig. 3A–C). These findings indicated that c.2T>G; p.M1R and c.5C>T; p.A2V mutations caused a remarkable reduction in ECHS1 protein expression. Notably, patient-derived and control myoblasts were similar with regard to *ECHS1* mRNA expression (Fig. 3D), indicating that the mutations apparently affected ECHS1 protein expression directly. Next, we measured ECHS1 enzyme activity in mitochondrial fractions prepared from patient-derived and control myoblasts. ECHS1 activity was normalized to CS activity, and activity in patient-derived myoblasts was 13% of that in control myoblasts (Fig. 3E). Therefore, the mutations caused a severe depletion of ECHS1 protein expression thereby decreasing ECHS1 enzyme activity.

To examine the stability of each mutated protein, we constructed three pIRES2-AcGFP1 expression plasmids, each expressed a different HA-tagged protein: wild-type, M1R-mutant, or A2V-mutant ECHS1. The expression of AcGFP was used as a transfection control. After the transfection into DLD-1 cells, immunoblotting of whole-cell lysate with anti-HA and GFP antibodies showed markedly higher expression of wild-type ECHS1 than of either mutant protein; all ECHS1 expression was normalized to AcGFP expression (Fig. 4, Supp. Fig. S2). This result indicated that ECHS1 protein expression was significantly reduced in the patient because of each mutation.

To confirm that the patient had ECHS1 deficiency, we performed a cellular complementation experiment. Patient-derived myoblasts had to be immortalized for these experiments because nonimmortalized cells exhibited poor growth and finite proliferation. The patient-derived myoblasts and control myoblasts were transfected with pEF321-T vector (a kind gift from Dr. Sumio Sugano, University of Tokyo). We then ascertained that ECHS1 protein expression and activity were lower in immortalized patient-derived myoblasts than in controls (Fig. 5A and B). We then transduced an empty expression vector, pEBMulti-Pur (Wako), or a pEBMulti-Pur construct containing a full-length, wild-type *ECHS1* cDNA into the immortalized patient-derived myoblasts; cells with the vector only or the ECHS1-expression construct are hereafter called vector-only and rescued myoblasts, respectively. ECHS1 protein expression level and enzyme activity were analyzed in mitochondrial fractions prepared from rescued myoblasts. Relative expression level of ECHS1 in rescued myoblasts was 11 times higher than that in vector-only myoblasts (Fig. 5A), and ECHS1 activity normalized to CS activity in rescued myoblasts was 49 times higher than that in vector-only myoblasts (Fig. 5B). From these cellular complementation experiments, we concluded the patient had ECHS1 deficiency.

Since the patient showed the combined mitochondrial respiratory chain deficiency in the skeletal muscle as mentioned above, we used a cellular complementation experiment to determine whether wild-type ECHS1 rescued the respiratory chain defect in patient-derived myoblasts. First, we measured enzyme activities of each mitochondrial respiratory complex in mitochondrial fractions prepared from immortalized patient-derived myoblasts. CS activity normalized values for complexes I, IV, and V activity in immortalized patient-derived myoblasts were decreased to 17%, 39%, and 43% of the mean values of immortalized control myoblasts (Fig. 5C). Then, we measured enzyme activity in mitochondrial fractions prepared from rescued myoblasts and found that each activity of complexes I, IV, and V was mostly restored relative to that in vector-only myoblasts. In rescued myoblasts, CS activity normalized values of complexes I, IV, and V were 3.5, 1.3, and 2.2 times higher than those in vector-only myoblasts (Fig. 5C). Mitochondrial respiratory complex activity was mostly restored in rescued myoblasts, suggesting that there was an unidentified link between deficiency of ECHS1 and respiratory chain.

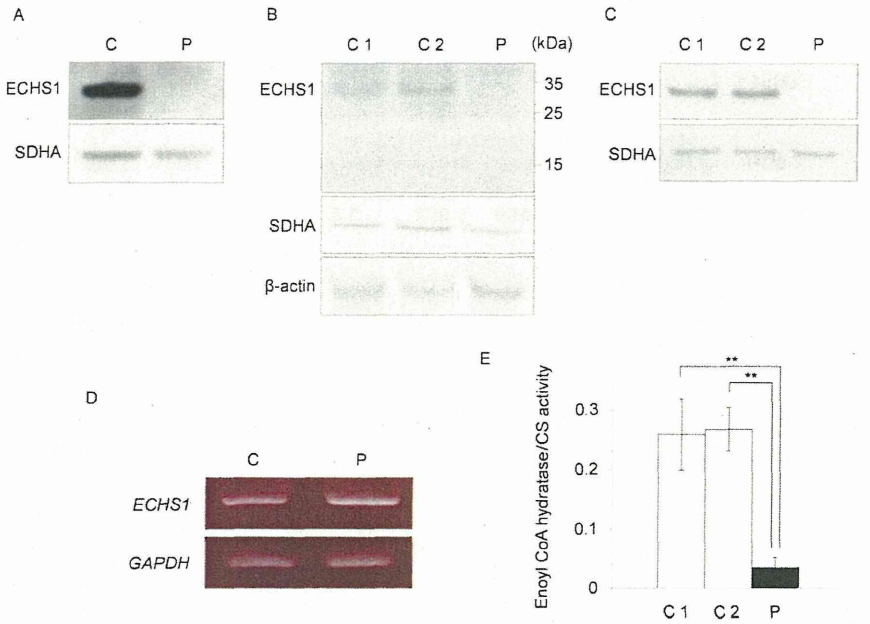

Figure 3. ECHS1 expression and enzyme activity. ECHS1 expression was analyzed by immunoblotting. C1/2, control; P, patient. Mitochondrial fraction prepared from patient's skeletal muscle (**A**) or whole-cell lysate (**B**) and mitochondrial fraction (**C**) prepared from the patient-derived myoblasts were analyzed via immunoblotting. All findings indicated that ECHS1 levels in patient samples were too low to detect by immunoblotting. **D**: RT-PCR was used to assess *ECHS1* mRNA levels in the patient. Notably, patient-derived myoblasts and control myoblasts did not differ with regard to *ECHS1* mRNA level. **E**: Mitochondrial fractions prepared from patient-derived myoblasts were used to estimate ECHS1 enzyme activity in the patient. All ECHS1 activity measurements were normalized to CS activity; ECHS1 activity in patient-derived samples was 13% of that in control samples. The experiments were performed in triplicate. Error bars represent standard deviations. (** $P < 0.005$ Student's *t*-test).

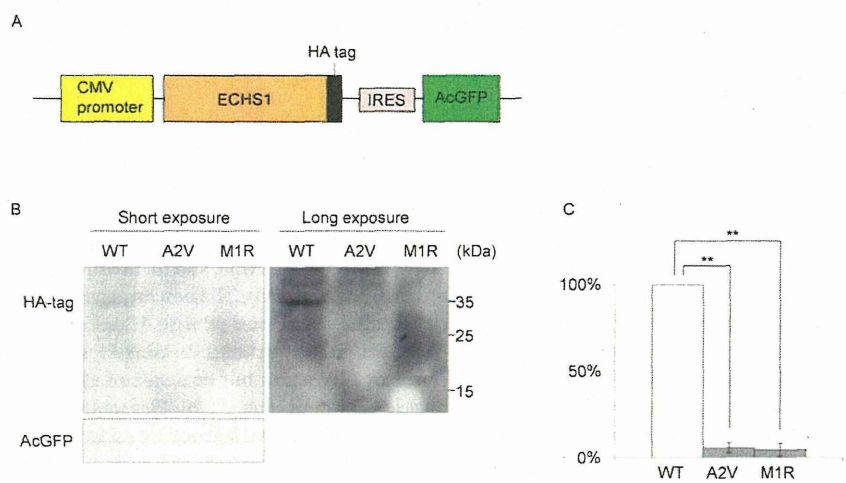

Figure 4. Exogenous expression of mutant ECHS1 protein in cancer cells. **A**: Schematic diagram of the pIRES mammalian expression vector. **B**: Representative image of an immunoblotting containing AcGFP, an internal control, and each HA-tagged ECHS1 protein; all proteins were isolated from DLD-1 cells that transiently overexpressed wild-type, A2V, or M1R HA-tagged ECHS1 from pIRES. The images obtained by short exposure (left) and long exposure (right). **C**: Overexpressed HA-tagged ECHS1 protein levels. Both mutant ECHS1 proteins showed dramatically decreased expression compared to wild-type ECHS1 protein, when ECHS1 was normalized relative to the internal control. Each experiment was performed in triplicate. Error bars represent standard deviations (** $P < 0.005$ Student's *t*-test).

Discussion

Here, we described a patient harboring compound heterozygous mutations in *ECHS1*. Immunoblotting analysis revealed that ECHS1 protein was undetectable in patient-derived myoblasts; moreover, these cells showed significantly lower ECHS1 enzyme activity than controls. Exogenous expression of two recombinant mutant proteins in DLD-1 cells showed c.2T>G; p.M1R and c.5C>T; p.A2V mutations affected ECHS1 protein expression. Cellular complementation experiment verified the patient had ECHS1 deficiency.

The c.2T>G; p.M1R mutation affected the start codon and therefore was predicted to impair the protein synthesis from canonical

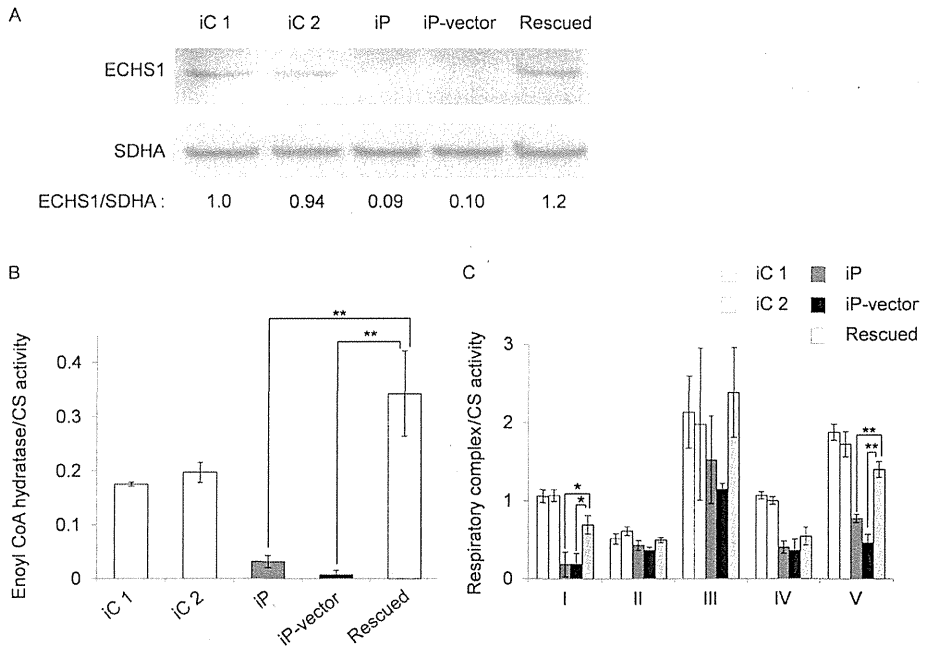

Figure 5. ECHS1 protein expression and enzyme activity in rescued myoblasts. An empty vector or a construct encoding wild-type ECHS1 was introduced into immortalized patient-derived myoblasts. iC1/2, immortalized control myoblasts; iP, immortalized patient-derived myoblasts; iP-vector, immortalized patient-derived myoblasts transfected with empty vector; Rescued, immortalized patient-derived myoblasts stably expressing wild-type ECHS1. **A:** ECHS1 levels were assessed on immunoblotting using mitochondrial fractions prepared from rescued myoblasts. ECHS1 level in "rescued" is 11 times higher than that in "iP-vector". **B:** Mitochondrial fractions prepared from rescued myoblasts were also used to measure ECHS1 enzyme activity. ECHS1 activity normalized to CS activity in "rescued" was 49 times higher than that in "iP-vector." Each experiment was performed in triplicate. Error bars represent standard deviations ($^{**}P < 0.005$ Student's *t*-test). **C:** Mitochondrial fractions prepared from rescued myoblasts were used to measure enzyme activities of mitochondrial respiratory complexes. Activity values were normalized to CS activity. Activities of complexes I, IV, and V were mostly restored from "iP" and "iP-vector." In "rescued," the enzyme activities of complexes I, IV, and V were 3.5, 1.3, and 2.2 times higher, respectively, than the "iP-vector." Each experiment was performed in triplicate. Error bars represent standard deviations ($^{**}P < 0.005$, $^{*}P < 0.05$ Student's *t*-test).

initiation site. In the reference *ECHS1* sequence, the next in-frame start codon is located in amino acids 97 (Fig. 2C). Even if translation could occur from this second start codon, the resulting product would lack the whole transit peptide and part of the enoyl-CoA hydratase/isomerase family domain (Fig. 2C). The c.5C>T; p.A2V mutation was located in the mitochondrial transit peptide and the mutation may affect the mitochondrial translocation of ECHS1. Surprisingly, the MitoProt-predicted mitochondrial targeting scores for the wild-type and A2V-mutant proteins were 0.988 and 0.991, respectively [MitoProt II; http://ihg.gsf.de/ihg/mitoprot.html; Claros and Vincens, 1996] and not markedly different from each other. Nevertheless, mislocalized mutant protein may have been degraded outside of the mitochondria. Consistent with this speculation was the finding that immunoblotting of lysate from patient-derived myoblasts (Fig. 3B) or from transfected cells that overexpressed the recombinant p.A2V-mutant ECHS1 (Fig. 4B, Supp. Fig. S2) did not show upper shifted ECHS1 bands that indicated ECHS1 with the transit peptide. Another possible explanation is that the mutation affected the translation efficiency because it was very close to the canonical start codon. It can change secondary structure of ECHS1 mRNA or alter the recognition by the translation initiation factors. As stated above, even if there was a translation product from the second in-frame start codon, that product would probably not function.

This patient presented with symptoms that are indicative of fatty acid oxidation disorders (e.g., hypotonia and metabolic acidosis), but he also presented with neurologic manifestations, including developmental delay and Leigh syndrome, that are not normally associated with fatty acid β-oxidation disorders. Interestingly, developmental delay is also found in cases of SCAD deficiency [Jethva et al., 2008]. In the absence of SCAD, the byproducts of butyryl-CoA—including butyrylcarnitine, butyrylglycine, ethylmalonic acid (EMA), and methylsuccinic acid—accumulate in blood, urine, and cells. These byproducts may cause the neurological pathology associated with SCAD deficiency [Jethva et al., 2008]. EMA significantly inhibits creatine kinase activity in the cerebral cortex of Wistar rats but does not affect levels in skeletal or heart muscle [Corydon et al., 1996]. Elevated levels of butyric acid modulated gene expression because excess butyric acid can enhance histone deacetylase activity [Chen et al., 2003]. Moreover, the highly volatile nature of butyric acid as a free acid may also add to its neurotoxic effects [Jethva et al., 2008].

On the other hand, it is very rare for fatty acid β-oxidation disorders causing Leigh syndrome. Therefore, the most noteworthy manifestation in this patient was Leigh syndrome. Leigh syndrome is a neuropathological entity characterized by symmetrical necrotic lesions along the brainstem, diencephalon, and basal ganglion [Leigh, 1951]. It is caused by abnormalities of mitochondrial energy generation and exhibits considerable clinical and genetic heterogeneity [Chol et al., 2003]. Commonly, defects in the mitochondrial respiratory chain or the pyruvate dehydrogenase complex are responsible for this disease. This patient's skeletal muscle samples exhibited a combined respiratory chain deficiency, and this deficiency may be the reason that he presented with Leigh syndrome. Although it

remained unclear what caused the respiratory chain defect, cellular complementation experiments showed almost complete restoration, indicating there was an unidentified link between ECHS1 and respiratory chain. One of the possible causes of respiratory chain defect is the secondary effect of accumulation of toxic metabolites. For example, an elevated urine glyoxylate was observed in this patient. Although the mechanism of this abnormal accumulation is not clear at the moment, it was shown that glyoxylate inhibited oxidative phosphorylation or pyruvate dehydrogenase complex by in vitro systems [Whitehouse et al., 1974; Lucas and Pons, 1975]. Therefore, we speculate that in our patient, ECHS1 deficiency induced metabolism abnormality including glyoxylate accumulation, and glyoxylate played a role in decreased enzyme activities of respiratory chain complexes. Interestingly, a recent paper describing patients with Leigh syndrome and ECHS1 deficiency showed decreased activity of pyruvate dehydrogenase complex in fibroblasts [Peters et al., 2014], (Supp. Table S5). BN-PAGE showed the assembly of respiratory complex components in the patient was not clearly different from the control (Supp. Fig. S1). This result suggests that the respiratory chain defect in the patient is more likely because of the secondary effect of accumulation of toxic metabolites. On the other hand, many findings indicate interplays between mitochondrial fatty acid β-oxidation and the respiratory chain. For example, Enns et al. [2000] mentioned the possibility of the physical association between these two energy-generating pathways from overlapping clinical phenotypes in genetic deficiency states. More recently, Wang and his colleagues actually showed physical association between mitochondrial fatty acid β-oxidation enzymes and respiratory chain complexes (Wang et al., 2010). Similarly, Narayan et al. demonstrated interactions between short-chain 3-hydroxyacyl-CoA dehydrogenase (SCHAD) and several components of the respiratory chain complexes including the catalytic subunits of complexes I, II, III, and IV via pull-down assays involving several mouse tissues. Considering the role of SCHAD as a NADH-generating enzyme, this interaction was suggested to demonstrate the logical physical association with the regeneration of NAD through the respiratory chain [Narayan et al., 2012]. Still more recently, mitochondrial protein acetylation was found to be driven by acetyl-CoA produced from mitochondrial fatty acid β-oxidation [Pougovkina et al., 2014]. Because the activities of respiratory chain enzymes are regulated by protein acetylation [Zhang et al., 2012], this finding indicated that β-oxidation regulates the mitochondrial respiratory chain. Remarkably, acyl-CoA dehydrogenase 9 (ACAD9), which participates in the oxidation of unsaturated fatty acid, was recently identified as a factor involved in complex I biogenesis [Haack et al., 2010; Heide et al., 2012]. Cellular complementation experiments that involve overexpression of wild-type ACAD9 in patient-derived fibroblast cell lines showed restoration of complex I assembly and activity [Haack et al., 2010]. Accumulating evidence indicates that there are complex regulatory interactions between mitochondrial fatty acid β-oxidation and the respiratory chain.

ECHS1 has been shown to interact with several molecules outside the mitochondrial fatty acid β-oxidation pathway [Chang et al., 2013; Xiao et al., 2013] and the loss of this interaction can affect respiratory chain function in a patient. Further functional analysis of ECHS1 will advance our understanding of the complex regulation of mitochondrial metabolism.

Acknowledgments

We acknowledge the technical support of Dr. Ichizo Nishino, Dr. Ikuya Nonaka, Dr. Chikako Waga, Takao Uchiumi, Yoshie Sawano, and Michiyo Nakamura. We also thank Dr. Sumio Sugano (the University of Tokyo) for providing the pEF321-T plasmid.

Disclosure statement: The authors have no conflict of interest to declare.

References

Chang Y, Wang SX, Wang YB, Zhou J, Li WH, Wang N, Fang DF, Li HY, Li AL, Zhang XM, Zhang WN. 2013. ECHS1 interacts with STAT3 and negatively regulates STAT3 signaling. FEBS Lett 587:607–613.

Chen JS, Faller DV, Spanjaard RA. 2003. Short-chain fatty acid inhibitors of histone deacetylases: promising anticancer therapeutics? Curr Cancer Drug Targets 3:219–236.

Chol M, Lebon S, Bénit P, Chretien D, de Lonlay P, Goldenberg A, Odent S, Hertz-Pannier L, Vincent-Delorme C, Cormier-Daire V, Rustin P, Rötig A, et al. 2003. The mitochondrial DNA G13513A MELAS mutation in the NADH dehydrogenase 5 gene is a frequent cause of Leigh-like syndrome with isolated complex I deficiency. J Med Genet 40:188–191.

Claros MG, Vincens P. 1996. Computational method to predict mitochondrially imported proteins and their targeting sequences. Eur J Biochem 241:779–786.

Corydon MJ, Gregersen N, Lehnert W, Ribes A, Rinaldo P, Kmoch S, Christensen E, Kristensen TJ, Andresen BS, Bross P, Winter V, Martinez G, et al. 1996. Ethylmalonic aciduria is associated with an amino acid variant of short chain acyl-coenzyme A dehydrogenase. Pediatr Res 39:1059–1066.

Enns GM, Bennett MJ, Hoppel CL, Goodman SI, Weisiger K, Ohnstad C, Golabi M, Packman S. 2000. Mitochondrial respiratory chain complex I deficiency with clinical and biochemical features of long-chain 3-hydroxyacyl-coenzyme A dehydrogenase deficiency. J Pediatr 136:251–254.

Ensenauer R, He M, Willard JM, Goetzman ES, Corydon TJ, Vandahl BB, Mohsen A-W, Isaya G, Vockley J. 2005. Human acyl-CoA dehydrogenase-9 plays a novel role in the mitochondrial beta-oxidation of unsaturated fatty acids. J Biol Chem 280:32309–32016.

Frezza C, Cipolat S, Scorrano L. 2007. Organelle isolation: functional mitochondria from mouse liver, muscle and cultured filroblasts. Nat Protoc 2:287–295.

Haack TB, Danhauser K, Haberberger B, Hoser J, Strecker V, Boehm D, Uziel G, Lamantea E, Invernizzi F, Poulton J, Rolinski B, Iuso A, et al. 2010. Exome sequencing identifies ACAD9 mutations as a cause of complex I deficiency. Nat Genet 42:1131–1134.

Heide H, Bleier L, Steger M, Ackermann J, Dröse S, Schwamb B, Zörnig M, Reichert AS, Koch I, Wittig I, Brandt U. 2012. Complexome profiling identifies TMEM126B as a component of the mitochondrial complex I assembly complex. Cell Metab 6:538–549.

Hochstrasser DF, Frutiger S, Paquet N, Bairoch A, Ravier F, Pasquali C, Sanchez JC, Tissot JD, Bjellqvist B, Vargas R, Ron DA, Graham JH. 1992. Human liver protein map: a reference database established by microsequencing and gel comparison. Electrophoresis 13:992–1001.

Ikeda Y, Dabrowski C, Tanaka K. 1983. Separation and properties of five distinct acyl-CoA dehydrogenases from rat liver mitochondria. J Biol Chem 258:1066–1076.

Ikeda Y, Hine DG, Okamura-Ikeda K, Tanaka K. 1985a. Mechanism of action of short-chain, medium chain and long-chain acyl-CoA dehydrogenases: direct evidence for carbanion formation as an intermediate step using enzyme-catalyzed C-2 proton/deuteron exchange in the absence of C-3 exchange. J Biol Chem 260: 1326–1337.

Ikeda Y, Okamura-Ikeda K, Tanaka K. 1985b. Spectroscopic analysis of the interaction of rat liver short chain, medium chain and long chain acyl-CoA dehydrogenases with acyl-CoA substrates. Biochemistry 24:7192–7199.

Jethva R, Bennett MJ, Vockley J. 2008. Short-chain acyl-coenzyme A dehydrogenase deficiency. Mol Genet Metab 95:195–200.

Kamijo T, Aoyama T, Miyazaki J, Hashimoto T. 1993. Molecular cloning of the cDNAs for the subunits of rat mitochondrial fatty acid beta-oxidation multienzyme complex. Structural and functional relationships to other mitochondrial and peroxisomal beta-oxidation enzymes. J Biol Chem 268:26452–26460.

Kim DW, Uetsuki T, Kaziro Y, Yamaguchi N, Sugano S. 1990. Use of the human elongation factor 1 alpha promoter as a versatile and efficient expression system. Gene 91:217–223.

Kompare M, Rizzo WB. 2008. Mitochondrial fatty-acid oxidation disorders. Semin Pediatr Neurol 15:140–149.

Leigh D. 1951. Subacute necrotizing encephalomyelopathy in an infant. J Neurol Neurosurg Psychiatr 14:216–221.

Lucas M, Pons AM. 1975. Influence of glyoxylic acid on properties of isolated mitochondria. Biochimie 57:637–645.

Matsunaga T, Kumanomido H, Shiroma M, Goto Y, Usami S. 2005. Audiological features and mitochondrial DNA sequence in a large family carrying mitochondrial A1555G mutation without use of aminoglycoside. Ann Otol Rhinol Laryngol 114:153–160.

Morava E, Rodenburg RJ, Hol F, de Vries M, Janssen A, van den Heuvel L, Nijtmans L, Smeitink J. 2006. Clinical and biochemical characteristics in patients with a high mutant load of the mitochondrial T8993G/C mutations. Am J Med Genet A 140:863–868.

Narayan, SB, Master SR, Sirec AN, Bierl C, Stanley PE, Li C, Stanley CA, Bennett MJ. 2012. Short-chain 3-hydroxyacyl-coenzyme A dehydrogenase associates with a protein super-complex integrating multiple metabolic pathways. PLoS One 7: e35048.

Peters H, Buck N, Wanders R, Ruiter J, Waterham H, Koster J, Yaplito-Lee J, Ferdinandusse S, Pitt J. 2014. ECHS1 mutations in Leigh disease: a new inborn error of metabolism affecting valine metabolism. Brain 137: 2903–2908.

Pougovkina O, Te Brinke H, Ofman R, van Cruchten AG, Kulik W, Wanders RJ, Houten SM, de Boer VC. 2014. Mitochondrial protein acetylation is driven by acetyl-CoA from fatty acid oxidation. Hum Mol Genet 23:3513–3522.

Shimazaki H, Takiyama Y, Ishiura H, Sakai C, Matsushima Y, Hatakeyama H, Honda J, Sakoe K, Naoi T, Namekawa M, Fukuda Y, Takahashi Y, et al. 2012. A homozygous mutation of C12orf65 causes spastic paraplegia with optic atrophy and neuropathy (SPG55). J Med Genet 49:777–784.

Spiekerkoetter U, Khuchua Z, Yue Z, Bennett MJ, Strauss AW. 2004. General mitochondrial trifunctional protein (TFP) deficiency as a result of either alpha- or beta-subunit mutations exhibits similar phenotypes because mutations in either subunit alter TFP complex expression and subunit turnover. Pediatr Res 55:190–196.

Steinman HM, Hill RL. 1975. Bovine liver crotonase (enoyl coenzyme A hydratase). Methods Enzymol 35:136–151.

Uchida Y, Izai K, Orii T, Hashimoto T. 1992. Novel fatty acid beta-oxidation enzymes in rat liver mitochondria. II. Purification and properties of enoyl-coenzyme A (CoA) hydratase/3-hydroxyacyl-CoA dehydrogenase/3-ketoacyl-CoA thiolase trifunctional protein. J Biol Chem 267:1034–1041.

Wang Y, Mohsen AW, Mihalik SJ, Goetzman ES, Vockley J. 2010. Evidence for physical association of mitochondrial fatty acid oxidation and oxidative phosphorylation complexes. J Biol Chem 285:29834–29841.

Whitehouse S, Cooper RH, Randle PJ. 1974. Mechanism of activation of pyruvate dehydrogenase by dichloroacetate and other halogenated carboxylic acids. Biochem J 141:761–774.

Xiao CX, Yang XN, Huang QW, Zhang YQ, Lin BY, Liu JJ, Liu YP, Jazag A, Guleng B, Ren JL. 2013. ECHS1 acts as a novel HBsAg-binding protein enhancing apoptosis through the mitochondrial pathway in HepG2 cells. Cancer Lett 330:67–73.

Zhang J, Lin A, Powers J, Lam MP, Lotz C, Liem D, Lau E, Wang D, Deng N, Korge P, Zong, NC, Cai H, et al. 2012. Perspectives on: SGP symposium on mitochondrial physiology and medicine: mitochondrial proteome design: from molecular identity to pathophysiological regulation. J Gen Physiol 139:395–406.

RESEARCH ARTICLE

AMERICAN JOURNAL OF medical genetics PART A

Mutations in *HADHB*, which Encodes the β-Subunit of Mitochondrial Trifunctional Protein, Cause Infantile Onset Hypoparathyroidism and Peripheral Polyneuropathy

Misako Naiki,[1,2] Nobuhiko Ochi,[3] Yusuke S. Kato,[4] Jamiyan Purevsuren,[5] Kenichiro Yamada,[1] Reiko Kimura,[1] Daisuke Fukushi,[1] Shinya Hara,[6] Yasukazu Yamada,[1] Toshiyuki Kumagai,[7] Seiji Yamaguchi,[5] and Nobuaki Wakamatsu[1]*

[1]Department of Genetics, Institute for Developmental Research, Aichi Human Service Center, Kasugai, Aichi, Japan

[2]Department of Pediatrics, Nagoya University Graduate School of Medicine, Nagoya, Aichi, Japan

[3]Department of Pediatrics, Daini-Aoitori Gakuen, Aichi Prefectural Hospital and Habilitation Center for Disabled Children, Okazaki, Aichi, Japan

[4]Institute for Health Science, Tokushima Bunri University, Tokushima, Japan

[5]Department of Pediatrics, Shimane University, Faculty of Medicine, Izumo, Shimane, Japan

[6]Department of Pediatrics, Toyota Memorial Hospital, Toyota, Aichi, Japan

[7]Department of Pediatric Neurology, Kobato Gakuen, Aichi Human Service Center, Kasugai, Aichi, Japan

Manuscript Received: 18 July 2013; Manuscript Accepted: 16 December 2013

Mitochondrial trifunctional protein (MTP) is a hetero-octamer composed of four α- and four β-subunits that catalyzes the final three steps of mitochondrial β-oxidation of long chain fatty acids. *HADHA* and *HADHB* encode the α-subunit and the β-subunit of MTP, respectively. To date, only two cases with MTP deficiency have been reported to be associated with hypoparathyroidism and peripheral polyneuropathy. Here, we report on two siblings with autosomal recessive infantile onset hypoparathyroidism, peripheral polyneuropathy, and rhabdomyolysis. Sequence analysis of *HADHA* and *HADHB* in both siblings shows that they were homozygous for a mutation in exon 14 of *HADHB* (c.1175C>T, [p.A392V]) and the parents were heterozygous for the mutation. Biochemical analysis revealed that the patients had MTP deficiency. Structural analysis indicated that the A392V mutation identified in this study and the N389D mutation previously reported to be associated with hypoparathyroidism are both located near the active site of MTP and affect the conformation of the β-subunit. Thus, the present patients are the second and third cases of MTP deficiency associated with missense *HADHB* mutation and infantile onset hypoparathyroidism. Since MTP deficiency is a treatable disease, MTP deficiency should be considered when patients have hypoparathyroidism as the initial presenting feature in infancy.

Key words: hypoparathyroidism; MTP deficiency; HADHB; LCKT; peripheral polyneuropathy

How to Cite this Article:
Naiki M, Ochi N, Kato YS, Purevsuren J, Yamada K, Kimura R, Fukushi D, Hara S, Yamada Y, Kumagai T, Yamaguchi S, Wakamatsu N. 2014. Mutations in *HADHB*, which encodes the β-subunit of mitochondrial trifunctional protein, cause infantile onset hypoparathyroidism and peripheral polyneuropathy.
Am J Med Genet Part A 164A:1180–1187.

Conflict of Interest: The authors declare no conflict of interests.
Grant sponsor: Takeda Science Foundation; Grant sponsor: Health Labor Sciences Research Grant; Grant sponsor: Ministry of Education, Culture, Sports, Science, and Technology of Japan (to N.W.); Grant number: #21390319.

Abbreviations: MTP, mitochondrial trifunctional protein; PTH, parathyroid hormone; LCEH, long-chain enoyl-CoA hydratase; LCHAD, long-chain 3-hydroxyacyl-CoA dehydrogenase; LCKT, long-chain 3-ketoacyl-CoA thiolase; CMT, Charcot-Marie-Tooth; MCAD, medium-chain acyl-CoA dehydrogenase.

*Correspondence to:
Nobuaki Wakamatsu, M.D., Ph.D., Department of Genetics, Institute for Developmental Research, Aichi Human Service Center, 713-8 Kamiya-cho, Kasugai, Aichi 480-0392, Japan.
E-mail: nwaka@inst-hsc.jp

Article first published online in Wiley Online Library (wileyonlinelibrary.com): 24 March 2014
DOI 10.1002/ajmg.a.36434

INTRODUCTION

MTP is a hetero-octamer composed of four α- and four β-subunits and contains three different enzyme activities that catalyze the final three chain-shortening reactions in the β-oxidation of long-chain fatty acids [Uchida et al., 1992]. *HADHA* encodes the α-subunit, which has both long-chain enoyl-CoA hydratase (LCEH, EC 4.2.1.17) and long-chain 3-hydroxyacyl-CoA dehydrogenase (LCHAD, EC 1.1.1.211) activities, whereas *HADHB* encodes the β-subunit, which has only long-chain 3-ketoacyl-CoA thiolase (LCKT, EC 2.3.1.16) activity [Uchida et al., 1992]. Mutations in *HADHA* or *HADHB* cause MTP (LCEH, LCHAD, LCKT) deficiency, with decreased activity and levels of all three enzymes because of the failure of hetero-octamer formation; however, a homozygous mutation (1528G>C) in *HADHA* has been reported to cause an isolated LCHAD deficiency [IJlst et al., 1994]. MTP deficiency is characterized by a wide range of clinical features, including cardiomyopathy, hypoketonic hypoglycemia, metabolic acidosis, sudden infant death, metabolic encephalopathy, liver dysfunction, peripheral neuropathy, exercise-induced myoglobinuria, and rhabdomyolysis [Wanders et al., 1999].

Hypoparathyroidism is a rare disorder characterized by hypocalcemia and hyperphosphatemia and is caused by deficiency in parathyroid hormone (PTH) action. An epidemiological survey showed that the prevalence of idiopathic hypoparathyroidism in Japan is 1:140,000 [Nakamura et al., 2000]. Impaired secretion of PTH causes PTH-deficient hypoparathyroidism, while resistance to PTH due to a defect in the PTH receptor or insensitivity to PTH results in pseudohypoparathyroidism. Autosomal recessive forms of isolated hypoparathyroidism have been reported to be caused by mutations in *PTH*, located on chromosome 11p15 [Parkinson and Thakker, 1992] or the gene encoding the parathyroid-specific transcription factor glial cells missing B (*GCMB*) on 6p24 [Ding et al., 2001].

Here, we report that two siblings born to consanguineous parents have MTP deficiency associated with infantile onset hypoparathyroidism. We have identified a new missense mutation in *HADHB* located close to the active site of the β-subunit of MTP. We also review hypoparathyroidism caused by MTP deficiencies and discuss the pathogenesis of the disease associated with hypoparathyroidism.

PATIENTS AND METHODS

Written informed consent was obtained from the patients and the family members who participated in this study. The experiments were conducted after approval by the institutional review board at the Institute for Developmental Research, Aichi Human Service Center.

The proband (IV-1) is an 18-year-old female born to first-cousin parents as a dizygotic twin (Fig. 1A). She was born at 37 weeks and 4 days gestation by normal vaginal delivery following an uneventful pregnancy. She was hospitalized 5 weeks after birth because of generalized seizures. Biochemical analysis revealed a decreased serum calcium concentration of 1.15 mmol/L (normal range: 2.25–2.75 mmol/L) and an elevated serum phosphorus concentration of 3.49 mmol/L (normal range: 1.21–2.18 mmol/L). The serum concentration of intact-PTH (iPTH) was below detectable levels (<5 pg/ml; normal range: 10–65 pg/ml). The concentrations of serum creatinine and blood urea nitrogen (BUN) were 0.3 mg/dl (normal range: 0.1–0.4 mg/dl) and 7 mg/dl (normal range: 7–19 mg/dl), respectively; thus, renal function was normal. She was diagnosed with hypoparathyroidism and was treated with activated vitamin D and calcium. The therapy elevated the serum calcium concentration, and she no longer experienced seizures. At 1 year of age, her serum calcium concentration had increased to 2.00 mmol/L, but her serum iPTH concentration was undetectable (<5 pg/ml). She achieved all developmental milestones at the appropriate age. At 2 years, she was admitted to the hospital with tetany after an upper respiratory tract infection. Upon admission, laboratory examination revealed an elevated serum creatine kinase concentration of 9,577 U/L (normal range: 20–150 U/L) and a low serum calcium concentration of 1.48 mmol/L. She was diagnosed with rhabdomyolysis and hypocalcemia and was successfully treated with intravenous fluids. She was later admitted to the hospital with recurrent episodes of fever, hypocalcemia, rhabdomyolysis, and myoglobinuria for several years. She has also experienced distal lower limb muscle weakness and atrophy since 3 years of age. Because of having a drop foot, she has had difficulty walking and has used foot orthoses or a wheelchair since she was 9. A neurologic examination at 9 years of age demonstrated distal muscle weakness, particularly involving the peroneal muscles, with absent tendon reflexes. There were no signs of pyramidal tract involvement. The motor conduction velocity of the peroneal nerve was decreased to 21.6 m/sec (normal range: 40–65 m/sec). Sensory conduction velocity of the sural nerve could not be evoked. The Gower's sign was negative. Thus, she has peripheral sensorimotor polyneuropathy. A muscle biopsy from the left biceps brachii demonstrated denervation atrophy with a predominance of type I fibers. She currently presents with severe muscular atrophy of the lower legs and hands with an absence of Achilles and patellar tendon reflexes, which are the clinical features of Charcot-Marie-Tooth (CMT) disease. She also has a drop foot and hammer toes, and touch and vibration senses of the distal legs are diminished (Fig. 1B). The serum calcium and iPTH concentrations at present were 2.10 mmol/L and 5 pg/ml, respectively. Analysis of blood acylcarnitines and urine organic acids measured once in a non-acute phase showed no abnormalities.

Patient IV-2 is an 18-year-old male who is the dizygotic twin of Patient IV-1 (Fig. 1A). Because his twin sister had hypoparathyroidism at the age of 1 month, his serum concentration of iPTH was measured at 4 months. He was asymptomatic, but his serum iPTH concentration was undetectable (<5 pg/ml) with a decreased calcium concentration (1.50 mmol/L) and an elevated phosphorus concentration (3.97 mmol/L). He started a regimen of activated vitamin D and calcium. He did not experience seizures but developed progressive peripheral polyneuropathy, and has exhibited rhabdomyolysis triggered by fevers from viral infections since he was 3. At 9 years of age, the motor conduction velocity of the peroneal nerve was decreased to 35.6 m/sec, and sensory conduction velocity of the sural nerve was not evoked. Findings from a muscle biopsy performed at 10 years of age were similar to those obtained for his sister. At 10 years of age, he required ventilator support owing to respiratory failure following an episode of rhab-

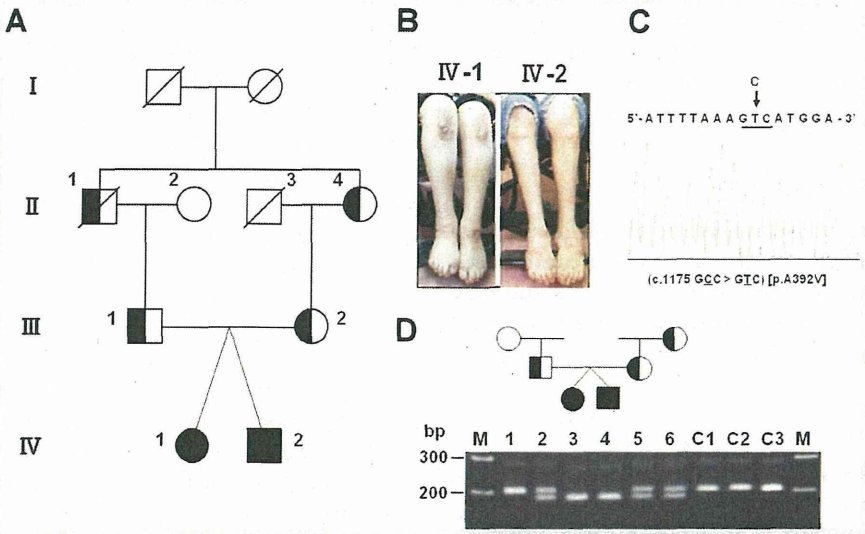

FIG. 1. The identification of the mutation in *HADHB*. A: The pedigree of the family with hypoparathyroidism and peripheral polyneuropathy. Affected individuals are indicated by filled symbols, unaffected individuals by unfilled symbols, and carrier individuals by half-filled symbols. B: The patients have muscle atrophy of the lower legs and deformity of the toes [hammer toes]. C: The direct sequence analysis of the patient IV-1 revealed a C to T substitution at nucleotide position 1175 in exon 14 of *HADHB*, resulting in the substitution of alanine [GCC] at codon 392 with valine [GTC] [c.1175C>T, [p.Ala392Val]], as indicated by the arrow. D: PCR-RFLP analysis using *Bsp*HI-digested PCR products from family members and three normal controls [C1, C2, and C3] were run through a 1.5% low-melting agarose gel. The sizes of the DNA markers are indicated on the left side.

domyolysis and myoglobinuria with a decreased calcium concentration (1.88 mmol/L) and a normal phosphorus concentration (1.93 mmol/L); however, his renal function was normal, as indicated by his serum creatinine (0.3 mg/dl) and BUN (17 mg/dl) concentrations. Analysis of blood acylcarnitines and urine organic acids in a non-acute phase showed no abnormalities. The serum calcium and iPTH concentrations at present were 2.20 mmol/L and 6 pg/ml, respectively. He currently presents with clinical features similar to those of his sister (Fig. 1B).

Patient IV-1 developed seizures due to hypoparathyroidism at 5 weeks after birth, and hypoparathyroidism was diagnosed in Patient IV-2 at the age of 4 months. Thus, both patients presented with infantile onset hypoparathyroidism. The clinical features of the presented patients are summarized in Table I.

DNA Analysis

Genomic DNA was isolated from white blood cells by phenol/chloroform extraction. Specific primers were designed to amplify *PTH*, *GCMB*, *HADHA*, and *HADHB*. PCR-amplified DNA fragments were isolated, purified, and sequenced using the Big Dye Terminator Cycle Sequencing Kit (Applied Biosystems, Foster City,

TABLE I. Clinical and Molecular Features of Hypoparathyroidism Associated With MTP Deficiency

Patients	**1**	**2**	**3**	**4**
Gender	Female	Female	Female	Male
Age at onset				
Hypoparathyroidism	15 m	4 m	5 w	4 m
Rhabdomyolysis	15 m	15 m	2 y	3 y
Peripheral polyneuropathy	15 m	4 m	3 y	3 y
Hypotonia	+	+	–	–
Liver dysfunction	+	+	–	–
HADHA/HADHB mutation	ND	N389D (HADHB)	A392V (HADHB)	A392V (HADHB)
References	Dionisi-Vici et al. [1996]	Labarthe et al. [2006]	This study	This study

+, present; –, not present; ND, not described; w, week; m, month; y, year.